IIETA International Information and Engineering Technology Association
Advancing the World of Information and Engineering

Journal of New Materials for Electrochemical Systems
Vol. 24, No.4, October 2021, pp. 278-283
Journal homepage: http://iieta.org/journals/jnmes

Di-metal element substitution of Al^{3+} and Ti^{4+} in Improving Electrochemical and Structural Behavior of Ceramic Solid Electrolytes

H. Rusdi[1*], N.S. Mohamed[1], R.H.Y Subban[2,3] and R. Rusdi[3*]

[1]Centre for Foundation Studies in Science, University of Malaya, 50603 Kuala Lumpur, Malaysia
[2]Faculty of Applied Sciences, Universiti Teknologi MARA, 40450 Shah Alam, Selangor, Malaysia
[3]Centre for Nanomaterials Research, Institute of Science, Level 3 Block C, Universiti Teknologi MARA, 40450 Shah Alam, Selangor, Malaysia

Corresponding Author Email: gireesh218@gmail.com

https://doi.org/10.18280/jnmes.v24i4.a07

Received: March 31-2021
Accepted: September 30-2021

Keywords:
NASICON; Mechanical milling; Glass ceramic electrolyte; Dielectric; Electrochemical.

ABSTRACT

Mechanical milling method is performed to prepare $Li_{1+x}Al_xTi_xSn_{2-2x}P_3O_{12}$ (x = 0.2, 0.4, 0.6, 0.8) NASICON-based ceramic solid electrolyte at 650 °C. X-ray diffraction (XRD) showed that $Li_{1.4}Al_{0.4}Ti_{0.4}Sn_{1.2}P_3O_{12}$ has almost pure compound that is isostructural to $LiSn_2(PO_4)_3$ and the addition of Al^{3+} and Ti^{4+} have reduced the cell volume of the electrolytes. Side occupancy factor studies verified that the electrolyte with x = 0.4 possessed Sn:Ti:Al ratio close to the theoritical ratio. Field emission scanning electron microscopy analysis portrayed that all electrolytes have flaky type morphology. From electrochemical impedance spectroscopy (EIS) analysis, the highest value achieved is 4.74×10^{-6} S cm^{-1} at x = 0.4. The substitutions of di-metal have affected the bulk resistance of the electrolytes. Dielectric constant of the electrolyte is at maximum when x = 0.4. The electrolytes follow non-Debye behavior as it shows a variation of relaxation times.

1. INTRODUCTION

Most researchers and engineers are rapidly changing their direction towards energy storage solutions e.g. lithium-ion battery and supercapacitor due to growing awareness about the environmental impacts of fossil fuels as well as resilience of energy grids around the world. Lithium batteries storage mechanism is usually dependent on the electrochemical reaction between electrolyte and electrodes. Lithium-ion batteries are used in various application such as automotive, aviation, electrical appliances and smart devices [1, 2]. Ceramic solid electrolyte (CSE) has many great advantages including high mechanical strength, excellent thermal stability together with electrochemical stability. These unique characteristics enable CSE to be useful in machines that require high durable materials [3, 4]. The use of CSE can eliminate several disadvantages e.g. solvent evaporation, leakage, corrosion and flammability [5].

Typically, CSE is a great Li-ion conductor compared to polymer and polymer/composite electrolytes due to the presence of channels in which alkaline ions can migrate easily [6]. This advantage can improve the capacity of a batteries and ionic mobility in the electrolyte. CSE also possesses better mechanical strength than polymer electrolyte. Some polycrystalline electrolytes that are classified under CSE are perovskite-type which is a calcium titanium oxide mineral composed of calcium titanate (CaTiO3) [7], garnet-type for example Li7La3Zr2O12 [8], sulfide-type like Li3PS4 and Li4SnS4 [9], argyrodite-type for example Li6PS5Br [10] and NASICON-type like LiZr2(PO4)3 system [11]. Other types of CSE has amorphous structure instead of regular crystalline structure. Most popular amorphous CSE used are LiPON-type or lithium phosphorus oxynitride [12] and lithium thiophosphates (Li2S–P2S5) [13].

The performance of NASICON-type is strongly dependent on the materials and composition used in the framework. This is because the parent compound, LiM2(PO4)3 can be altered to various possible structures where M can be tin (Sn), titanium (Ti), germanium (Ge), hafnium (Hf) or zirconium (Zr) [14]. The PO4 tetrahedron and MO6 octahedron in NASICON structure acts as channels for alkali ions to move from one electrode to another [15]. As reported by other researchers [16-18], LiSn2P3O12 has a great electrical and thermal stability and can withstand shock and pressure. However, LiSn2P3O12 usually has a low conductivity value. This obstacle can be solved by substitution method using trivalent cation like gallium (Ga), indium (In), yttrium (Y), aluminium (Al), vanadium (V), iron (Fe), chromium (Cr) or scandium (Sc). In this work, di-metal element substitution method has been implemented using Al3+ and Ti4+. Hence the new formula after di-metal element substitution is Li1+xAlxTixSn2-2xP3O12 where x is varied from 0.2 to 0.8. The substitution process creates positive charge deficiency which is compensated by Li-ion [19].

2. EXPERIMENTAL PROCEDURE

2.1. Materials

Lithium oxide (Li2O, 99%), tin (IV) oxide (SnO2, 98%), ammonium dihydrogen phosphate (NH4H2PO4, 98%), titanium (IV) Oxide (TiO2, 99.8%) and aluminium oxide (Al2O3, 99.99%) were procured from Aldrich.

2.2. Synthesis OF LI1+XALXTIXSN2-2XP3O12

Starting materials e.g. SnO2, Li2O, TiO2, NH4H2PO4 and Al2O3 were grinded and mixed using a planetary ball miller. The mixture was then placed in an alumina crucible and heated at 700 ºC for 2 hours. The pre-heating process was performed to eliminate H2O and NH4 from NH4H2PO4 to gain P2O5 [3]. The resultant mixtures were inserted into a bowl filled with zirconium (Zr) balls. The milling process was conducted using a Fristch 7 ball mill at 500 rpm for 80 hours. The mixture was pressed at 7 ton of pressure using Specac Hydraulic Press to form pellets. The thickness of the pellets were from 1 to 13 mm. Different sintering temperatures such as 550, 650, 750, 850 and 950 oC were used for 8 hours. This process is crucial to determine the best conductivity value. It was found that for each x value, the optimum conductivity was obtained at sintering temperature of 650 oC. The designation of the samples were B2, B4, B6 and B8 for x = 0.2, 0.4, 0.6 and 0.8, respectively. To remove excess moisture in or on the pellets, desiccators containing SiO2 gel was used to store the final pellets.

Bruker AXS D8 Advance X-ray Diffraction spectrometer (Cu-K radiation, 1.5406 Å) was employed to study the phase and structural properties of the pellets in 2θ range between 10o and 90 o. The structure of Li1+xAlxTixSn2-2xP3O12 were matched with the R-3c space group of LiSn2P3O12. Xpert HighScore Plus software was used to conduct structural studies by refinement method.

Solartron SI 1260 Impedance Analyzer was used to conduct electrochemical impedance spectroscopy (EIS) in the frequency range of 1 Hz to 32 MHz. The value of conductivity (□) from impedance spectra was obtained using the equation below:

$$\sigma = \frac{d}{R_{bulk} A} \qquad (1)$$

where d stands for the thickness of the pellet, Rbulk is the bulk resistance and A is the interfacial contact area between the electrode and electrolyte. JEOL 7600F FESEM was used to capture the surface morphology of the samples. The samples were examined under vacuum condition with accelerating voltage of 3 kV and magnification of 20k×.

Apart from conductivity, EIS analysis can also provide the dielectric properties of a system. Dielectric analysis was used to portray the capacitive behavior of the electrolyte and to confirm the pattern of conductivity. Charge stored in the electrolyte is called dielectric constant (□') while the dissipation of energy is called as dielectric loss (□''). Data from impedance analysis has been used to obtain dielectric parameters. ε' and ε'' which are expressed as [20]:

$$\varepsilon' = \frac{Z''}{\omega C_o \left(Z'\right)^2 + \omega C_o \left(Z''\right)^2} \qquad (2)$$

$$\varepsilon'' = \frac{Z'}{\omega C_o \left(Z'\right)^2 + \omega C_o \left(Z''\right)^2} \qquad (3)$$

where, Z' and Z" are the real (x-axis) and imaginary (y-axis) part of the impedance. Co is the vacuum capacitance and ω stands for angular frequency.

Ionic-conducting behavior of a material was examined via electrical modulus analysis. The real and imaginary parts of modulus are M' and M'', respectively, where M' and M'' can be expressed as:

$$M' = \frac{\left(\varepsilon'\right)^2}{\left(\varepsilon'\right)^2 + \left(\varepsilon''\right)^2} \qquad (4)$$

$$M'' = \frac{\left(\varepsilon''\right)^2}{\left(\varepsilon'\right)^2 + \left(\varepsilon''\right)^2} \qquad (5)$$

From the peak in the plot of M'', relaxation time (t_{rex}) was determined using the following equation:

$$t_{rex}\omega_{peak} = 1 \qquad (6)$$ where ω_{peak} is the angular frequency of the relaxation peak.

3. RESULT AND DISCUSSION

3.1. XRD analysis

XRD analysis has been used to study the structural properties of each electrolyte. Fig. 1 shows the XRD diffractograms for all samples that have been sintered at 650 ºC. Diffraction peaks in all samples show the peaks are corresponding to $LiSn_2(PO_4)_3$ with the ICDD reference pattern number 01-087-2078 which is reported in [21]. It can be observed that B4 has almost pure compound due its pattern that is isostructural to $LiSn_2(PO_4)_3$ [21]. The lattice parameters and the cell volume of each electrolyte have been analyzed by means of the Rietveld refinement via Xpert HighScore Plus software using the structural ICSD reference 83831. The extracted lattice parameters of all samples are tabulated in Table 1. The cell volume (V) of all samples is smaller compared to LSP. The decrease in the lattice parameters is due to smaller ionic radius of Al^{3+} (0.57 Å) and Ti^{4+} (0.605 Å) compared to Sn^{4+} (0.65 Å). The theoretical ratio of Sn:Ti:Al is 0.6:0.2:0.2. By comparing the side occupancy factor (s.o.f) of each electrolyte, it is observed that the Sn:Ti:Al ratio in B4 sample has the nearest value to the theoretical value which is 0.63:0.19:0.17. This result is consistent with the conductivity result where B4 has the highest conductivity which is discussed next.

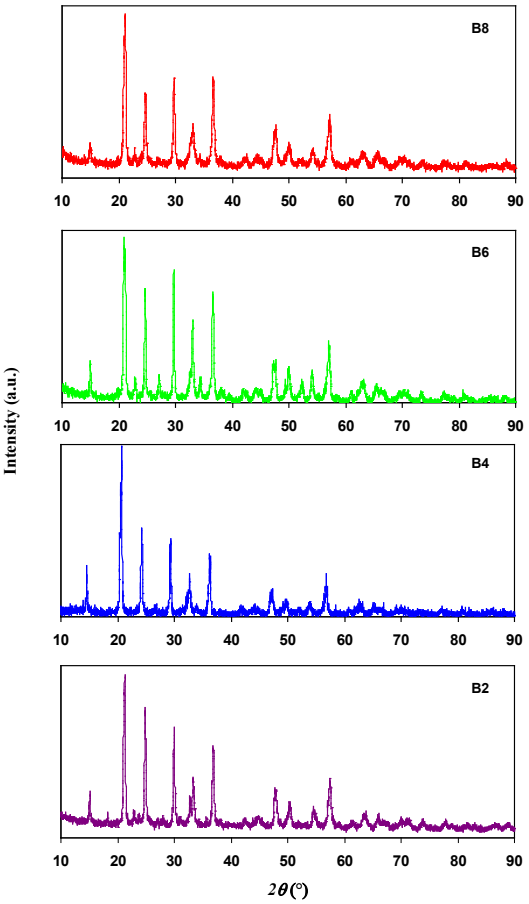

Figure 1. XRD diffractograms of $Li_{1+x}Al_xTi_xSn_{2-x}P_3O_{12}$ (x = 0.2, 0.4, 0.6, 0.8) sintered at 650 °C

3.2. Electrochemical study

Fig. 2 shows the Nyquist plot of $Li_{1+x}Al_xTi_xSn_{2-2x}P_3O_{12}$ where x = 0.2, 0.4, 0.6, 0.8 at 650 °C. The value of R_{bulk} for this kind of plot is taken from the meeting point of the titled line and the semicircle. The semicircle at higher frequency region is due to conduction of ions in the bulk of the electrolyte while the tilted line at low frequency indicates polarization effects [22]. It is noticeable that the bulk resistance of the electrolyte is reduced and is the smallest when x = 0.4. As the amount of substituent increases, the bulk resistance is observed to increase. The highest conductivity achieved is 4.74×10^{-6} S cm^{-1} when x = 0.4 (Table 2). According to Bae et al. [23], the highest conductivity achieved for $Li_7La_3Zr_2O_{12}$ system is 1.09×10^{-6} S cm^{-1}. Rao et al. [24] stated that the differences in conductivity are typically related to the connectivity between grains, which have a higher concentration of imperfections near the grain boundary. The authors reported a similar trend of conductivity variation where the highest conductivity value is 4.25 x 10^{-6} S cm^{-1} for $LiTi_2(PO_4)_3$ system. The inclusion of x = 0.4 of Al^{3+} has optimized the conductivity to 2.5 x 10^{-6} S cm^{-1} for $Li_{1+x}Al_xSn_{1.2+x}P_3O_{12}$ based solid electrolyte which is reported by Lu et al. [25]. Thus, $Li_{1.4}Al_{0.4}Ti_{0.4}Sn_{1.2}P_3O_{12}$ has a conductivity value that is higher or comparable to other ceramic electrolyte-based studies. When the cell volume increased, ion can move easily in the cell which in turn enhanced the conductivity values. However, too large volume can lead to conductivity decrement as ions require more energy to move to neighboring sites.

Table 1. Lattice parameters of $Li_{1+x}Al_xTi_xSn_{2-x}P_3O_{12}$ (x = 0.2, 0.4, 0.6, 0.8).

Sample	*a*(=*b*) /Å	*c* (Å)	*V* (Å^3)	*c*/*a*	R_w	χ^2	s.o.f of Li in 6b	s.o.f of Sn in 12c	s.o.f of Ti in 12c	s.o.f of Al in 12c	s.o.f of P in 3b	s.o.f of O
LSP (83831)	8.63	21.53	1389.82	2.49	-	-	-	-	-	-	-	-
B2	8.55	21.54	1337.82	2.52	24.2	4.57	1.00	0.61	0.29	0.09	0.82	1.00
B4	8.57	21.35	1359.32	2.49	40.12	1.41	1.00	0.63	0.19	0.17	0.97	1.00
B6	8.57	21.35	1359.32	2.49	17.35	2.53	0.80	0.90	0.20	0.19	1.00	0.93
B8	8.58	21.40	1365.20	2.49	16.79	2.09	1.00	0.60	0.25	0.11	0.82	0.94

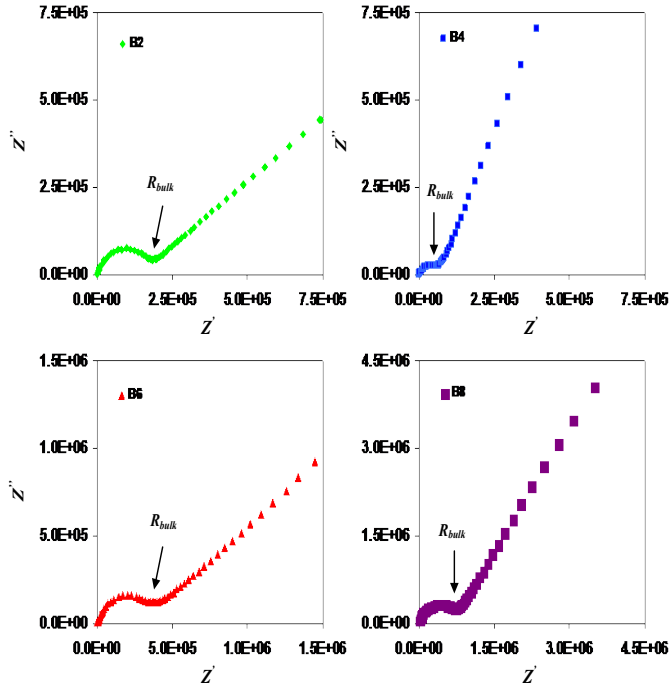

Figure 2. Nyquist plot of the $Li_{1+x}Al_xTi_xSn_{2-2x}P_3O_{12}$ (x = 0.2, 0.4, 0.6, 0.8) sintered at 650 °C

Table 2. Conductivity values for each electrolyte sintered at 650 °C.

Electrolyte	Conductivity value, σ (S cm^{-1})
B2	4.08×10^{-6}
B4	4.74×10^{-6}
B6	1.41×10^{-6}
B8	1.41×10^{-7}

3.3. Surface morphology study

Further investigation has been conducted to study the surface morphology of the sample. Fig. 3 portrays the surface of $Li_{1+x}Al_xTi_xSn_{2-2x}P_3O_{12}$ (x = 0.2, 0.4, 0.6, 0.8). It shows that the samples obtained are irregular in shape and some are with flaky type of morphology with high agglomeration. There are also some samples which have spherical-like shape. Based on Fig. 3, the particle size distributions of all the samples are found to be homogeneous. However, among all compositions, B4 has the most consistent particle size distribution while B2, B6 and B8 have some large crystal structures. The pathway of ions and electrons to conduct is easier in compound with homogenous particle size distribution [26, 27]. This result concurred with those of XRD and conductivity analysis.

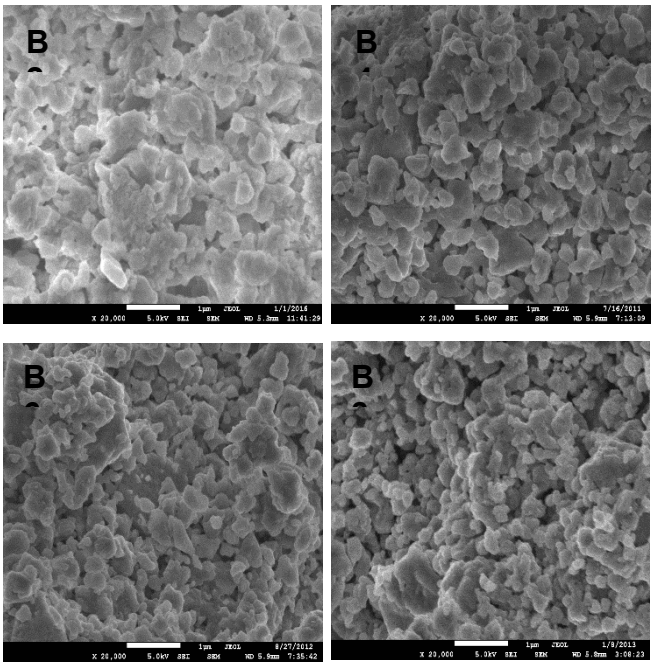

Figure 3. FESEM micrograph of the $Li_{1+x}Al_xTi_xSn_{2-2x}P_3O_{12}$ (x = 0.2, 0.4, 0.6, 0.8) sintered at 650 °C

3.4. Dielectric analysis

Dielectric analysis is a crucial method to identify ionic transport and phase transition mechanism in a system. The plot of ε' versus frequency is displayed in Fig. 4 where it has a same trend as ε'' in Fig. 5. Both ε' and ε'' are high at low frequency region. As observed in Fig. 4, the value of ε' is low at high frequency region (Log $f > 3$). Rao et al. [24] reported that polarization takes place at low frequency as ions can form a proper charge double layer at the surface of the electrode. ε' is observed to approach zero as Log f goes beyond 3. At rapid rate of electrical flow, charge carriers experience unstable flow including collision among charge carries which disabled a proper formation of charge double-layer [28-30]. The value of ε' is at maximum when x = 0.4. Thus, it can be proven that in $Li_{1+x}Al_xTi_xSn_{2-2x}(PO_4)_3$, the number of charge carriers is the largest when x = 0.4. The trend of conductivity in Table 2 is further verified as it is consistent with the trend of ε' in Fig. 4.

The loss of energy of $Li_{1+x}Al_xTi_xSn_{2-2x}(PO_4)_3$ (x = 0.2 to 0.8) at 650 °C are shown in Fig. 5. The value of ε'' for sample with x = 0.4 is at maximum and it dropped as x value changes to 0.2, 0.6 and 0.8. This portrays that $Li_{1.4}Al_{0.4}Ti_{0.4}Sn_{1.2}(PO_4)_3$ has more free ions or charge carriers compared to other compositions. More energy loss is observed as more ionic collision occurs. The pattern of dielectric constant and loss in this study is similar to other NASICON-based solid electrolyte reported in the literature [24, 31]. These authors stated that their NASICON-based electrolytes have the behavior of an ionic conductor.

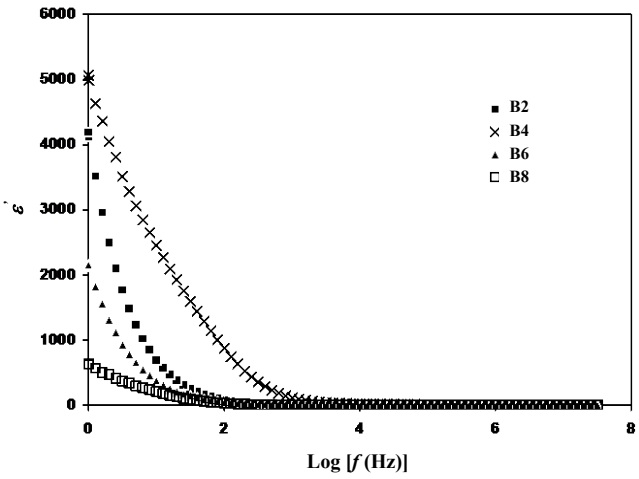

Figure 4. Variation of $e^{'}$ different frequencies for $Li_{1+x}Al_xTi_xSn_{2-2x}(PO_4)_3$ (x = 0.2, 0.4, 0.6 0.8) at 650 °C

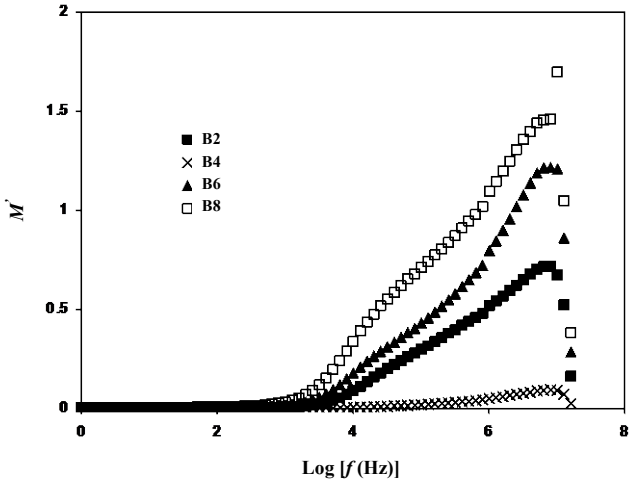

Figure 6. Variation of $M^{'}$different frequencies for $Li_{1+x}Al_xTi_xSn_{2-2x}(PO_4)_3$ (x = 0.2, 0.4, 0.6 0.8) at 650 °C

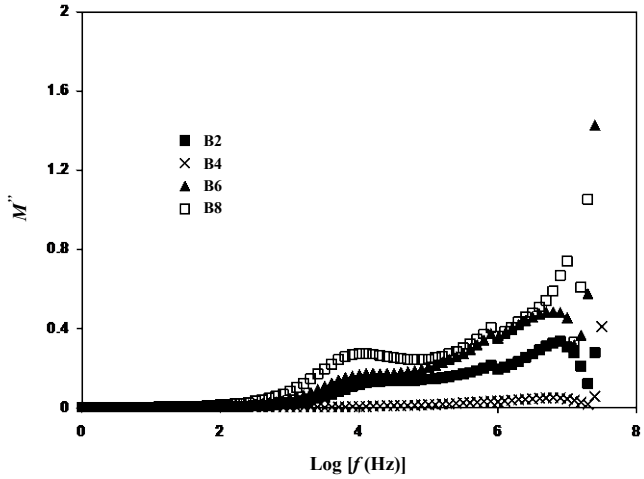

Figure 5. Variation of $e^{''}$ different frequencies for $Li_{1+x}Al_xTi_xSn_{2-2x}(PO_4)_3$ (x = 0.2, 0.4, 0.6 0.8) at 650 °C

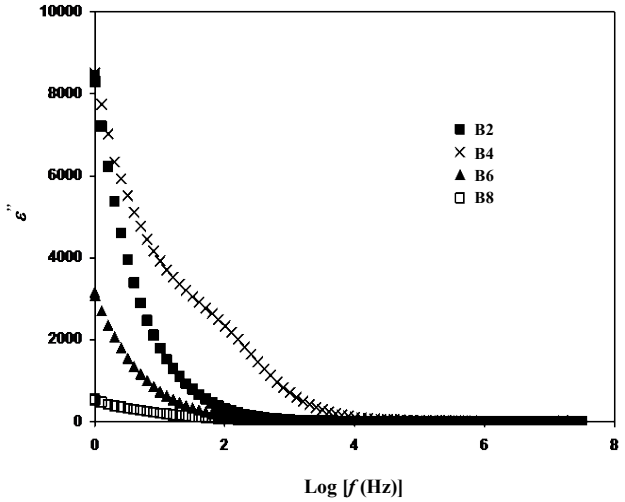

Figure 7. Variation of $M^{''}$different frequencies for $Li_{1+x}Al_xTi_xSn_{2-2x}(PO_4)_3$ (x = 0.2, 0.4, 0.6 0.8) at 650 °C

3.5. Electrical modulus analysis

The electrical properties of the composite material $Li_{1+x}Al_xTi_xSn_{2-2x}(PO_4)_3$ (x=0.2, 0.4, 0.6, 0.8) NASICON-type is further studied using electrical modulus which analyses the response of lithium Li^+ ions due to the presence of electric field. $M^{'}$ is used to examine ionic conductivities in correlation with the ionic process and conductivity relaxation. It is noticed that the pattern of $M^{'}$ in Fig. 6 possesses peak at ~ Log f = 7 for all compositions. The presence of this peak is common in a conductor of ion. Relaxation process is usually located at the high frequency region while conduction process at low frequency region [32]. The value of $M^{'}$ shows that it is low and almost approaching zero from Log f = 0 to Log f = 3. Tripathi et al. [33] reported that at low frequency region, electrode polarization is dominant. It can be verified that $Li_{1.4}Al_{0.4}Ti_{0.4}Sn_{1.2}(PO_4)_3$ has the highest charge carrier amount compared to other composition due to its low $M^{'}$ value. This outcome tallies with the results of conductivity in Table 2.

Figure 7 illustrates the effect of frequency on $M^{''}$. The peak of $M^{''}$ shifted towards higher frequency from x = 0.2 to x = 0.4 and shifted back towards lower frequency regions for x = 0.6 and 0.8. Nikam and Deshpande [34] stated that variation of relaxation of charge carriers signifies that the system follows non-Debye type of behavior. This outcome is similar to the NASICON type structure reported by Arumugam et al. [35] with $Li_{1.3}Al_{0.3}Ti_{1.7}(PO_4)$ system. The t_{rex} of each electrolyte is tabulated in Table 3. t_{rex} is 1.98×10^{-8} s for the chosen x value of 0.2 and it reduced to 1.57×10^{-8} s when x = 0.4. The trend of t_{rex} concurred with the trend of conductivity. The presence of relaxation is due to free ions having to follow the alteration in electric field direction.

Table 3. Relaxation for $Li_{1+x}Al_xTi_xSn_{2-2x}(PO_4)_3$ (x = 0.2, 0.4, 0.6 0.8).

Electrolyte	t_{rex} (s)
B2	1.98×10^{-8}
B4	1.57×10^{-8}
B6	2.49×10^{-8}
B8	1.57×10^{-5}

4. CONCLUSION

$Li_{1+}xAlxTixSn2_{-2x}P_3O_{12}$ (x = 0.2 to 0.8) solid electrolyte materials have been prepared using mechanical milling method at 650 °C for 8 h. $Li_{1.4}Al_{0.4}Ti_{0.4}Sn_{1.2}P_3O_{12}$ has been discovered to be almost pure compound which is similar to $LiSn_2(PO_4)_3$. The small radius of Al^{3+} and Ti^{4+} are the reason of electrolyte cell volume decrement. Sn:Ti:Al ratio is found to be 0.63:0.19:0.17 when x = 0.4. This ratio is almost consistent with the theoritical ratio of Sn:Ti:Al which is 0.6:0.2:0.2. Field emission scanning electron microscope (FESEM) showed a flaky type structure with high agglomeration and the size distribution is the best at x = 0.4. The maximum conductivity value obtained is 4.74×10^{-6} S cm^{-1} for $Li_{1.4}Al_{0.4}Ti_{0.4}Sn_{1.2}P_3O_{12}$. The dielectric properties of the electrolytes are dependent on frequency and tallied with the results of conductivity. The electrolytes in this work obeys non-Debye behavior as it illustrates a variation of relaxation times.

ACKNOWLEDGEMENT

The authors would like to thank University of Malaya and Universiti Teknologi MARA for the facilities provided.

REFERENCE

[1] S. Fewa, O. Schmidta, G.J. Offer, N. Brandon, J. Nelsona, A. Gambhira, Energy Pol., 114, 578 (2018).
[2] Y. Kato, S. Hori, T. Saito, K. Suzuki, M. Hirayama, A. Mitsui, M. Yonemura, H. Iba, R. Kanno, Nat. Energy, 1, 16030 (2016).
[3] G.F. Ortiz, M.C. López, P. Lavela, C. Vidal-Abarca, J.L. Tirado, Solid State Ionics, 262, 573 (2014).
[4] M. Botros, T. Scherer, R. Popescu, A. Kilmametov, O. Clemens, H. Hahn, RSC Adv., 9, 31102 (2019).
[5] C. Chi, Y. Li, D. Li, H. Huang, Q. Wang, Y. Yang, B.J. Huang, Mater. Chem., A7, 16748 (2019).
[6] L. Qinghui, X. Chang, H. Bing, Y. Xin, Mater., 13, 1719 (2020).
[7] H. Bing, Z. Shengwen, L. Jiangbin, H. Zeya, W. Chang–An, J. Power Sources, 429, 75 (2019).
[8] L. Liansheng, D. Yuanfu, C. Guohua, J. Energy Chem., 50, 154 (2020).
[9] M. Otoyama, A. Sakuda, M. Tatsumisago, A. Hayashi, ACS Appl. Mater. Interfaces, 26, 29228 (2020).
[10] Z. Zhuoran, Z. Jianxing, J. Huanhuan, P. Linfeng, A. Tao, X. Jia, J. Power Sources, 450, 227601 (2020).
[11] M. Harada, H. Takeda, S. Suzuki, K. Nakano, N. Tanibata, M. Nakayama, M. Karasuyama, I. Takeuchi, J. Mater. Chem., A 8, 15103 (2020).
[12] A.S. Rudyi, M.E. Lebedev, A.A. Mironenko, L.A. Mazaletskii, V.V. Naumov, A.V. Novozhilova, I.S. Fedorov, A.B. Churilov, Russ. Microelectron, 49, 345-357 (2020).
[13] F. Strauss, H.T. Jun, J. Janek, T. Brezesinski, Inorg. Chem. Front., 7, 3953-3960 (2020).
[14] H. El-Shinawi, A. Regoutz, D.J. Payne, H.J. Cussen, S.A. Corr, J. Mater. Chem., A 6, 5296 (2018).
[15] M. Guin, F. Tietz, O. Guillon, Solid State Ionics, 293, 18 (2016).
[16] R. Norhaniza, R.H.Y. Subban, N.S. Mohamed, A. Ahmad, Int. J. Electrochem. Sci., 7, 10254 (2012).
[17] R. Norhaniza, R.H.Y. Subban, N. S. Mohamed, J. Mat. Sci., 46, 7815 (2011).
[18] M. G. Lazarraga, J. Ibañez, M. Tabellout, J.M. Rojo, Compos. Sci. Technol., 64, 759 (2004).
[19] B. Lang, B. Ziebarth, C. Elsässer, Chem. Mater., 27, 5040 (2015).
[20] A. Arya, M. Sadiq, A.L. Sharma, Mater. Today, 12, 554 (2019).
[21] H. Rusdi, N. S. Mohamed, R.H.Y. Subban, AIP Conf. Pro., 1877, 050005 (2017).
[22] M.H. Hamsan, S.B. Aziz, M.M. Nofal, M.A. Brza, R.T. Abdulwahid, J.M. Hadi, W.O. Karim, M.F.Z. Kadir, J. Mater. Res. Tech., 9, 10635 (2020).
[23] J. Bae, S. J. Lee, J. T. Son, J. Korean Phys. Soc., 74, 187 (2019).
[24] M. K. Rao, K.V. Babu, V. Veeraiah, K.J. Samatha, Asian Ceram. Soc., 6, 109 (2018).
[25] X. Lu, H. Xiao, Ceram-Silik., 61, 14 (2017).
[26] R.O. Fuentes, F.M. Figueiredo, F.M.B. Marques, J.I. Franco, Solid State Ionics, 140, 173 (2001).
[27] A. Kumar, K. Shahi, Solid State Com., 94, 813 (1995).
[28] M. I. Kimpa, M.Z.H. Mayzan, J.A. Yabagi, M.M. Nmaya, K.U. Isah, M.A. Agam, IOP Conf. Ser. Earth Environ. Sci., 140, 012156 (2018).
[29] F. K. Tan, J. Hassan, Z. A. Wahab, Int. J. Eng. Sci. Technol., 19, 2081 (2016).
[30] S. B. Aziz, H.J. Woo, M.F.Z. Kadir, H.M.J. Ahmed, J. Sci. Adv. Mater. Dev., 3, 1 (2018).
[31] T. Zangina, J. Hassan, K.A. Matori, R.S. Azis, U. Ahmadu, A. See, Results Phys., 6, 719 (2016).
[32] A.F. Fuzlin, N.M.J. Rasali, A.S. Samsudin, Mater. Sci. Eng., 342, 012080 (2018).
[33] N. Tripathi, A. Shukla, A.K. Thakur, D.T. Marx, Polym. Eng. Sci., 60, 297 (2019).
[34] P. N. Nikam, V.D. Deshpande, Mater., Today 5, 2254 (2018).
[35] R. Arumugam, K.H. Prasad, N. Satyanarayana, E.S. Srinadhu, TechConnect., 2, 52 (2018).